Haldane and dimer gaps in general double-spin-chain models

1997 J. Phys.: Condens. Matter 9 6401

(http://iopscience.iop.org/0953-8984/9/30/009)

J. Phys.: Condens. Matter **9** (1997) 6401–6415. Printed in the UK PII: S0953-8984(97)82187-X

Haldane and dimer gaps in general double-spin-chain models

T Nakamura†, S Takada‡, K Okamoto§ and N Kurosawa†

† Department of Applied Physics, Tohoku University, Sendai, Miyagi 980-77, Japan
‡ Institute of Physics, University of Tsukuba, Tsukuba, Ibaraki 305, Japan
§ Department of Physics, Tokyo Institute of Technology, Oh-Okayama, Meguro, Tokyo 152, Japan

Received 25 February 1997

Abstract. We have obtained an analytic expression for the k-dependence of the excitation energy gap for an arbitrary double $S = 1/2$ spin chain by using the non-local unitary transformation and the variational method. We check that it explains the gap behaviour of various systems, which include the Haldane system and the dimer system in both extreme limits, and also the ladder model and the Majumdar–Ghosh model. The string order parameter, the dimer order parameter, and the local spin value are also calculated in the ground state. The ground-state energy exhibits a great stabilization by an antiferromagnetic bond dimerization, which might be realized in various new compounds. We also mention the relation of the convergence to the Haldane state with the spin-exchange symmetry of the model. The excited state has one domain wall of a local triplet type except in the vicinity of the Majumdar–Ghosh point, where a local triplet is decomposed into two $S = 1/2$ free spins moving among the singlet dimers.

1. Introduction

The low-dimensional quantum systems with excitation energy gaps have been attracting much interest both theoretically and experimentally [1], though the interest had only been from the theoretical side until recently. The simplest theoretical spin model may be the dimer model that consists of independent pairs of $S = 1/2$ spins connected by an antiferromagnetic (AF) interaction bond. The ground state is a product of a singlet dimer state on each bond, and the excitation gap is the singlet–triplet dimer gap. The Majumdar–Ghosh (M–G) model [2, 3] and the Δ chain model [4–6] also realize the perfect singlet dimer ground state, and thus the gap is intrinsically the dimer gap. Another well-known model that has a different origin of the gap is the $S = 1$ AF spin chain, the so-called Haldane system [7]. The ladder model [8–11] and the bond-alternation model [8, 12–14] interpolate between the dimer model and the Haldane system on changing the strength of the interaction bonds as a parameter from $+\infty$ to $-\infty$. Therefore, these models were investigated mainly to clarify the details of the Haldane system. Our understanding up to now is that the dimer state continuously changes to the $S = 1$ Haldane state without any explicit phase transition occurring [8–14]. On the other hand, the phase transition becomes of first order in a ladder model with both interactions diagonal [15].

The situation has changed now that it has become possible to synthesize various compounds that actually realize the above theoretical models [16–19]. For example, magnetic susceptibility measurements on $KCuCl_3$ [17] and on CaV_2O_5 [18] indicate a

0953-8984/97/306401+15$19.50

spin-gap behaviour, and the experimental data are considered to be explained through the frustrated double-spin-chain model [20]. In such an analysis, we need to estimate the gap as a function of the strength of the interaction bonds. Then the susceptibility can be calculated by using the gap value [21].

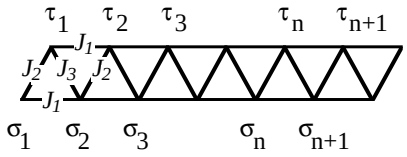

Figure 1. The shape of the general double-spin-chain model that we treat in this paper.

In this paper, we consider the generalized double-spin-chain system as defined by its next-nearest-neighbour interaction, J_1, and the alternating nearest-neighbour interactions, J_2 and J_3, as follows:

$$\mathcal{H} = \sum_{n=1}^{N} J_1(\boldsymbol{\sigma}_n \cdot \boldsymbol{\sigma}_{n+1} + \boldsymbol{\tau}_n \cdot \boldsymbol{\tau}_{n+1}) + J_2\boldsymbol{\sigma}_n \cdot \boldsymbol{\tau}_n + J_3\boldsymbol{\tau}_n \cdot \boldsymbol{\sigma}_{n+1}. \tag{1}$$

Here, N is the linear size of the system, and $|\boldsymbol{\sigma}| = |\boldsymbol{\tau}| = 1/2$. Figure 1 shows the lattice described. The system is reduced to the M–G model with a choice of parameter set $(J_1, J_2, J_3) = (0.5, 1, 1)$, the isotropic ladder model with $(J_1, J_2, J_3) = (1, 1, 0)$, or $(1, 0, 1)$, and the $S = 1$ AF chain in the limit $J_2 \to -\infty$. The case with $J_1 = 0$ corresponds to the bond-alternation model for a single chain. Recently, the string order parameter [22] and the energy for the ground state of this system have been calculated by the matrix-product method [23]. Here, we make use of the non-local unitary transformation [24–26], and give explicit expressions for the ground-state energy, the excitation gap, the string order parameter, the dimer order parameter, the local spin value in the ground state, and the domain wall spin value in the excited state for arbitrary (J_1, J_2, J_3). This transformation is an adaptation of the Kennedy–Tasaki transformation [24] of the $S = 1$ system to the $S = 1/2$ double-spin-chain systems, and is known to be powerful when the ground state is either in the Haldane state or in the state with strong dimer correlation.

In section 2, we introduce the transformation and the variational method employed in this paper. Then the energy, a local bond-spin value, and the order parameters for the ground state are estimated, and compared with the numerical diagonalization results for the $N = 12$ lattice. Section 3 describes the excited states, where we consider two types of variation. One is the local triplet domain wall excitation, for which we give an explicit form for the whole phase space. The other one is what we call the kink–antikink excitation, which is governed by two $S = 1/2$ free spins moving among the perfect singlet dimers [26, 27]. This type is the elementary excitation near the M–G point.

2. The ground state

We first rewrite the Hamiltonian, equation (1), using the non-local unitary transformation [24–26]. The transformation is defined by U in the following:

$$U = \prod_{n=1}^{N} U_n \tag{2}$$

$$U_n = P_n^+ + P_n^- \exp(\mathrm{i}\pi S_n^x) \tag{3}$$

$$P_n^{\pm} = \frac{1}{2}\left[1 \pm \exp\left(\mathrm{i}\pi \sum_{k=1}^{n-1} S_k^z\right)\right] \tag{4}$$

$$\boldsymbol{S}_n = \boldsymbol{\sigma}_n + \boldsymbol{\tau}_n \tag{5}$$

where P_n^+ (P_n^-) is the operator for projection onto states with the even (odd) numbers of $S_i^z = \pm 1$ for $i \leqslant n-1$. Then the Hamiltonian (1) is transformed as

$$\begin{aligned} U^{-1}\mathcal{H}U = \sum_{n=1}^{N} & J_1(-\sigma_n^x\tau_{n+1}^x - \tau_n^z\sigma_{n+1}^z - 4\sigma_n^x\tau_{n+1}^x\tau_n^z\sigma_{n+1}^z) \\ & + J_1(-\tau_n^x\sigma_{n+1}^x - \sigma_n^z\tau_{n+1}^z - 4\tau_n^x\sigma_{n+1}^x\sigma_n^z\tau_{n+1}^z) \\ & + J_3(-\tau_n^x\tau_{n+1}^x - \sigma_n^z\sigma_{n+1}^z - 4\tau_n^x\tau_{n+1}^x\sigma_n^z\sigma_{n+1}^z) + J_2\boldsymbol{\sigma}_n \cdot \boldsymbol{\tau}_n. \end{aligned} \tag{6}$$

We consider the following variational basis for the ground state of this Hamiltonian:

$$|\Psi_0\rangle = \prod_{n=1}^{N} |n(\alpha, \beta, \gamma, b)\rangle = \prod_{n=1}^{N} (b|T_n\rangle + \sqrt{1-b^2}|S_n\rangle) \tag{7}$$

$$|S_n\rangle = (|\uparrow, \downarrow\rangle - |\downarrow, \uparrow\rangle)/\sqrt{2} \tag{8}$$

$$|T_n\rangle = \alpha|\uparrow, \uparrow\rangle + \beta(|\uparrow, \downarrow\rangle + |\downarrow, \uparrow\rangle)/\sqrt{2} + \gamma|\downarrow, \downarrow\rangle. \tag{9}$$

The $|\uparrow, \uparrow\rangle$ are the states of $|\sigma_n^z, \tau_n^z\rangle$. b, α, β, and γ are the real variational parameters, and satisfy the normalization condition $\alpha^2 + \beta^2 + \gamma^2 = 1$. These parameters are supposed to be independent of n, since we consider the uniform ground state. In this sense, the present analysis is variational.

A state with $b = 0$ is a singlet dimer state on the $\boldsymbol{\sigma}_n$–$\boldsymbol{\tau}_n$ bond, a state with $b = \sqrt{3}/2$ is the other singlet dimer state on the $\boldsymbol{\sigma}_{n+1}$–$\boldsymbol{\tau}_n$ bond, and a state with $b = 1$ corresponds to the pure VBS state on the $\boldsymbol{\sigma}_n$–$\boldsymbol{\tau}_n$ bond. It should be noted that our approximation is not the single-site approximation for the original Hamiltonian, so the $\boldsymbol{\sigma}_{n+1}$–$\boldsymbol{\tau}_n$ dimer can be represented by equation (7) with $b = \sqrt{3}/2$.

The energy expectation value is calculated as

$$\begin{aligned} \langle\Psi_0|\frac{\mathcal{H}}{\mathcal{N}}|\Psi_0\rangle = {} & J_2\left(b^2 - \frac{3}{4}\right) - (2J_1 + J_3)b^4\left[\beta^2(\alpha^2 + \gamma^2) + \frac{(\alpha^2 - \gamma^2)^2}{4}\right] \\ & + (2J_1 - J_3)b^2(1 - b^2) - 3J_3b^3\sqrt{1-b^2}\beta(\alpha^2 - \gamma^2). \end{aligned} \tag{10}$$

We can easily find this minimum value under the constraint $\alpha^2 + \beta^2 + \gamma^2 = 1$, by using the Lagrange multiplier. The energy expectation value ϵ_0 is

$$\epsilon_0 = \left(J_2 - \frac{8}{3}b^2J_1\right)\left(b^2 - \frac{3}{4}\right) - \frac{b^2}{3}J_3(b + \sqrt{3(1-b^2)})^2 \tag{11}$$

with four possible choices of the parameters (α, β, γ) as follows:

$$(\alpha, \beta, \gamma) = (\pm\sqrt{2/3}, \sqrt{1/3}, 0), (0, -\sqrt{1/3}, \pm\sqrt{2/3}) \tag{12}$$

and b determined implicitly through

$$J_2 = \left(b^2 - \frac{3}{4}\right)\left(\frac{4}{3}(4J_1 - J_3) - \frac{4bJ_3}{\sqrt{3(1-b^2)}}\right) + 2J_1 \tag{13}$$

or

$$b = 0. \tag{14}$$

The fourfold degeneracy in the choice of (α, β, γ) corresponds to the degeneracy of the edge states [13, 25, 28]. A state with $b = 0$ is a trivial singlet dimer ground state at $J_2 = \infty$.

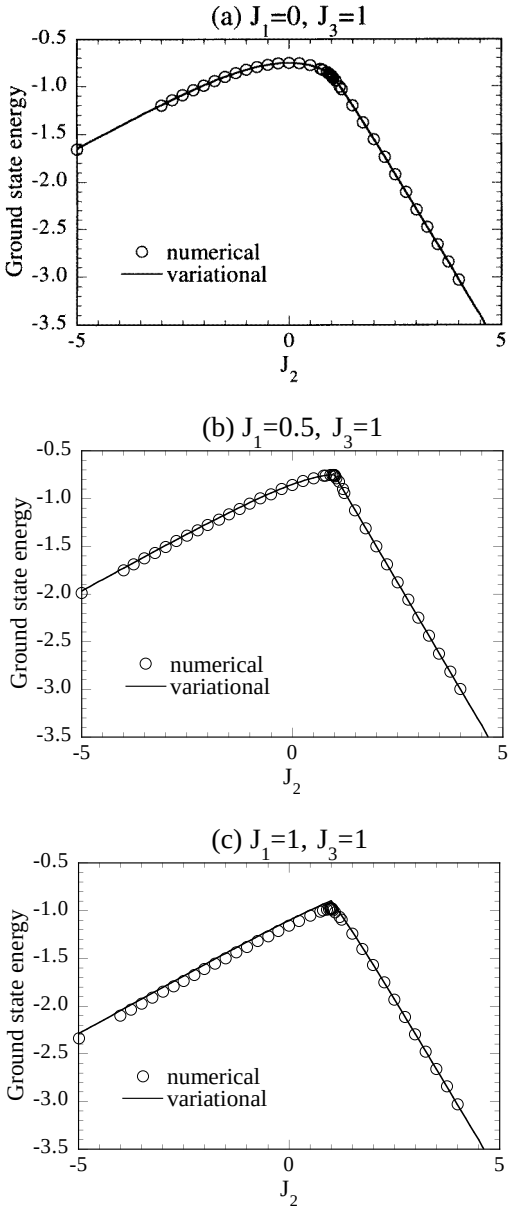

Figure 2. The ground-state energy for (a) $J_1 = 0$ and $J_3 = 1$ (the bond-alternation model), (b) $J_1 = 0.5$ and $J_3 = 1$ (including the M–G model at $J_2 = 1$), and (c) $J_1 = 1$ and $J_3 = 1$ (including the isotropic ladder model at $J_2 = 0$). Circles denote the numerical diagonalization results for $N = 12$, and lines show the variational estimates.

The other one, equation (13), represents a non-trivial state that will be the ground state for most of the parameter space. We solved equation (13) numerically by the bisection method for arbitrary (J_1, J_2, J_3).

Before going through the details of the following variational results, let us notice that the system possesses the symmetry which exchanges J_2-bonds and J_3-bonds. It does not

matter when we solve the eigenvalue problem exactly; however, the variational results are dependent upon this exchange. Therefore, we must do the same variational analysis on a system whose J_2-values and J_3-values are exchanged as well as on a system with a given parameter (J_1, J_2, J_3), and must compare the two sets of results. In the present analysis, the ground-state energy is always lower if we exchange J_2 and J_3 in the case where $J_2 > J_3$.

We consider three cases which only differ in the choice of J_1. J_3 is always set equal to 1, and J_2 is a variable that we move from $+\infty$ to $-\infty$. Case (a): $J_1 = 0$ and $J_3 = 1$ is the bond-alternation model. It includes the pure dimer model at $J_2 = 0$, and the uniform $S = 1/2$ AF spin chain at $J_2 = 1$. Case (b): $J_1 = 0.5$ and $J_3 = 1$ includes the M–G model at $J_2 = 1$. Case (c): $J_1 = 1$ and $J_3 = 1$ includes the isotropic ladder model at $J_2 = 0$. In addition, these three cases include a pure dimer model at $J_2 = +\infty$, and the $S = 1$ AF chain at $J_2 = -\infty$. Let us call the singlet dimer state on the J_2-bonds the J_2-singlet, and also that on the J_3-bonds the J_3-singlet hereafter, for simplicity.

Figure 2 shows the J_2-dependence of the ground-state energy, ϵ_0, compared with the numerical diagonalization results for a system with $N = 12$ under periodic boundary conditions. The variational estimates are made by exchanging J_2 and J_3 in the region $J_2 > J_3$. The energy agrees with the numerical values fairly well, particularly in the dimer region where $J_2 > J_3 = 1$. The difference becomes visible in the Haldane region ($J_2 < J_3 = 1$) as J_1 increases. The energy takes a maximum value at the fully frustrated point $J_2 = J_3 = 1$ in figures 2(b) and 2(c). As J_2 goes away from $J_3 = 1$, the energy decreases, because the frustration is relaxed. It should be noted that this energy stabilization is stronger in the dimer region as compared with the Haldane region. Thus, we point out here the possibility that the ground states of the real double-spin-chain compounds are also easily stabilized to the dimer ground state by a lattice dimerization similar to the spin–Peierls system corresponding to the case shown in figure 2(a).

Next, we calculate the local bond-spin value, defined by

$$\langle S(J_2)\rangle = \left\langle \boldsymbol{\sigma}_n \cdot \boldsymbol{\tau}_n + \frac{3}{4} \right\rangle = b^2 \tag{15}$$

$$\langle S(J_3)\rangle = \left\langle \boldsymbol{\sigma}_{n+1} \cdot \boldsymbol{\tau}_n + \frac{3}{4} \right\rangle = -\frac{b^2}{3}(b + \sqrt{3(1-b^2)})^2 + \frac{3}{4}. \tag{16}$$

Here, $S(J_i)$ denotes the local spin expectation value along the J_i-bond. Since a local bond-spin value is not a good quantum number, we have to define it by using a projection operator which selects the local triplet component from the composite spin magnitude. The bond correlation $\boldsymbol{\sigma}_n \cdot \boldsymbol{\tau}_n + 3/4$ serves as this projection operator for $S(J_2)$. $S(J_i)$ takes the value zero for the J_i-singlet state, while the other bond spin takes a value of $3/4$.

Figure 3 shows the J_2-dependence of $S(J_2)$ and $S(J_3)$. The lines show the variational estimates stated above, and the symbols show the numerical diagonalization results for $N = 12$.

Consistency between the variational estimates and the numerical results is generally excellent, except for $S(J_3)$ of figure 3(c). In figure 3(a), i.e. the bond-alternation model, there are two trivial pure dimer points. The ground state is the J_2-singlet state at $J_2 = +\infty$, and is the J_3-singlet state at $J_2 = 0$. These two points are equivalent to each other if we exchange the J_2-bonds and the J_3-bonds. Thus, the local bond-spin values are symmetric about the isotropic point at $J_2 = 1$, where the model reduces to the uniform $S = 1/2$ AF spin chain. The J_3-singlet state continuously changes to the Haldane state in the limit of $J_2 \to -\infty$, as is manifested by $S(J_2)$ converging to 1. In the model that includes the M–G model, figure 3(b), the ground state is exactly the J_2-singlet for $J_2 > 1$, where $S(J_2) = 0$ and $S(J_3) = 3/4$. $S(J_2)$ and $S(J_3)$ show a sudden jump at $J_2 = 1$, since the J_3-singlet is

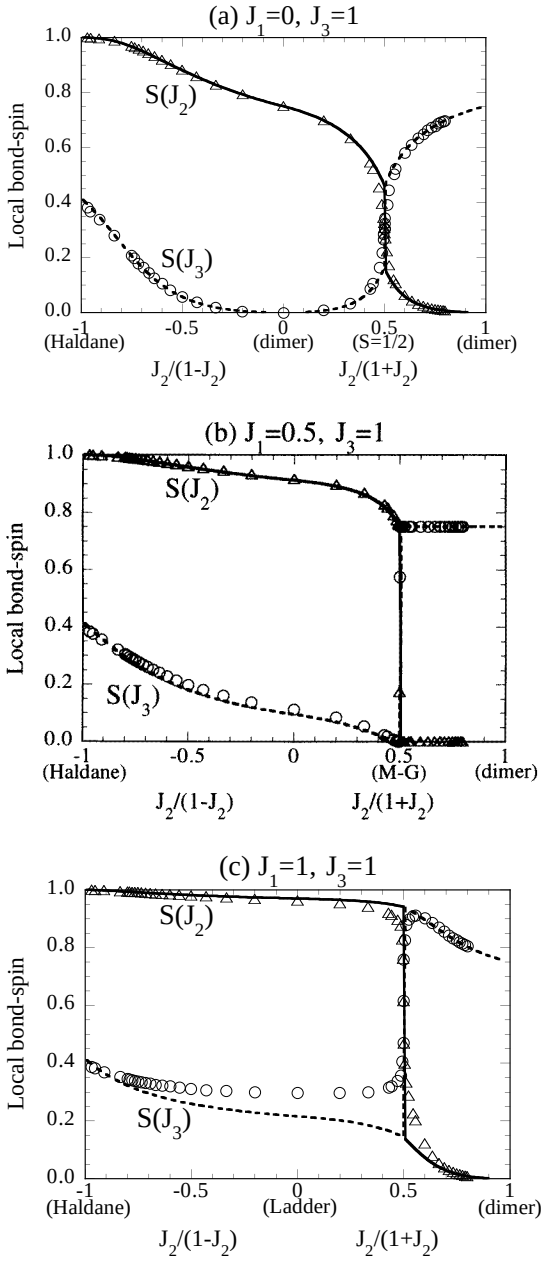

Figure 3. The local bond-spin value on the J_2-bond ($S(J_2)$) and that on the J_3-bond ($S(J_3)$) plotted against $J_2/(1-J_2)$ for $J_2 < 0$, and against $J_2/(1+J_2)$ for $J_2 > 0$, where (a) $J_1 = 0$ and $J_3 = 1$ (the bond-alternation model), (b) $J_1 = 0.5$ and $J_3 = 1$ (including the M–G model at $J_2 = 1$), and (c) $J_1 = 1$ and $J_3 = 1$ (including the isotropic ladder model at $J_2 = 0$). The lines show the variational estimates. Triangles and circles show the numerical diagonalization results for $S(J_2)$ and $S(J_3)$ of a system with 24 spins under periodic boundary conditions.

degenerate with the J_2-singlet at this point. The situation is rather different in figure 3(c), since the J_3-singlet never becomes the ground state in this case. $S(J_3)$ increases from $3/4$

as J_2 decreases from $+\infty$, until it suddenly decreases at the symmetric point, $J_2 = J_3 = 1$. $S(J_2)$ now takes nearly the triplet value at $J_2 \sim 1$. At the isotropic ladder point where $J_2 = 0$, the diagonal spins of the ladder almost form a triplet state, since $S(J_2) \sim 1$, and the rung spins are far from the singlet state, since $S(J_3) \sim 0.3$.

We can also estimate the string order parameter of den Nijs and Rommelse, $O_{\rm str}$ [22], and the dimer order parameter, $O_{\rm dim}$, defined by Hida [12, 13]. They are

$$O_{\rm dim}(J_3) = \lim_{|m-n|\to\infty} -4\left\langle U^{-1}\tau^z_m \exp\left[\mathrm{i}\pi \sum_{k=m+1}^{n-1} S^z_k\right]\sigma^z_n U\right\rangle$$
$$= \lim_{|m-n|\to\infty} 4\langle\sigma^z_m\sigma^z_n\rangle = 4\langle\sigma^z_m\rangle^2 = \frac{4b^2}{9}(b+\sqrt{3(1-b^2)})^2 \tag{17}$$

$$O_{\rm str}(J_2) = \lim_{|m-n|\to\infty} -\left\langle U^{-1}S^z_m \exp\left[\mathrm{i}\pi \sum_{k=m+1}^{n-1} S^z_k\right]S^z_n U\right\rangle = \lim_{|m-n|\to\infty}\langle S^z_m S^z_n\rangle = \langle S^z_m\rangle^2 = \frac{4}{9}b^4. \tag{18}$$

In addition, $O_{\rm dim}(J_2) = 1$ only when $b = 0$, and otherwise it vanishes; $O_{\rm str}(J_3) = O_{\rm dim}(J_2)/4$.

Figure 4 shows the J_2-dependence of the dimer and the string order parameter in the ground states of the three cases mentioned above. Symbols denote the numerical diagonalization results for $N = 12$, and lines show the variational estimates. The order parameters both on the J_2-bonds and on the J_3-bonds are plotted in the same figure. For example, $O_{\rm str}(J_2)$ is defined by equation (18) when we consider the bond-spin $\boldsymbol{S}_n$ to be along the J_2-bond, and $O_{\rm str}(J_3)$ is defined with $\boldsymbol{S}_n$ along the J_3-bond. Hence, $O_{\rm str}(J_i)$ denotes the den Nijs–Rommelse string order as regards the triplet state of each J_i-bond. On the other hand, $O_{\rm dim}(J_i)$ expresses the dimer order on each J_i-bond. We exchanged J_2 and J_3 for $J_2 > J_3$, as mentioned before.

Consistency of the variational estimates with the numerical results is excellent, except in the limit of $J_2 \to -\infty$. The variation gives the pure VBS state, while the numerical results converge to the correct $S = 1$ value. This is because we used a single-site approximation of the transformed Hamiltonian in the variation, and therefore our estimates always become worse when the correlation length of the ground state is rather long, as is the case in the Haldane state. Positive values of $O_{\rm dim}(J_2)$ in the region $J_2 < J_3 = 1$ constitute the finite-size effect, and should vanish in the thermodynamic limit.

In the system of figure 4(a), i.e., the bond-alternation model, $O_{\rm dim} = 1$ at the two pure dimer points. The variational estimates are particularly good near these two points because of the short correlation length, while they become poor near the uniform $S = 1/2$ chain point at $J_2 = 1$ and the uniform $S = 1$ chain point at $J_2 = -\infty$.

In figure 4(b), $O_{\rm dim}(J_2)$ is 1 for $J_2 > 1$, since the ground state is exactly the J_2-singlet. $O_{\rm str}(J_2)$ and $O_{\rm dim}(J_3)$ are zero in this region. However, $O_{\rm str}(J_3)$ takes a finite value of $1/4$. This is a natural consequence of the definition of the string order parameter. Thus, it is not adequate to discriminate between the Haldane phase and the dimer phase on the basis of the vanishing or non-vanishing of this parameter alone. We should determine the phase from the value of this parameter, ranging from 1/4 in the dimer state to 0.37 in the Haldane state. Therefore, it is very difficult to draw a phase boundary line in most cases. As J_2 decreases from 1, the J_3-singlet remains the ground state by changing continuously towards the Haldane state in the limit of $J_2 \to -\infty$, as is observed in the behaviour of $O_{\rm dim}(J_3)$ and $O_{\rm str}(J_2)$.

The inconsistency between the variational estimates and the numerical results in

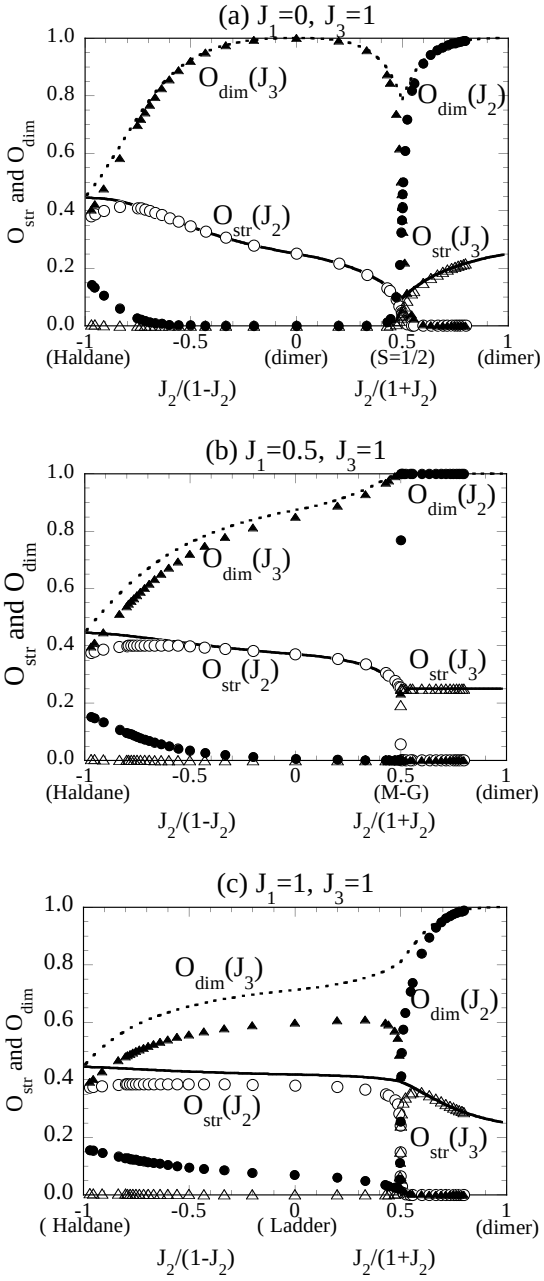

Figure 4. $O_{\rm str}$ and $O_{\rm dim}$ on the J_2-bonds (circles) and those on the J_3-bonds (triangles) are plotted against $J_2/(1-J_2)$ for $J_2<0$, and against $J_2/(1+J_2)$ for $J_2>0$, where (a) $J_1=0$ and $J_3=1$ (the bond-alternation model), (b) $J_1=0.5$ and $J_3=1$ (including the M–G model at $J_2=1$) and (c) $J_1=1$, and $J_3=1$ (including the isotropic ladder model at $J_2=0$). Solid (broken) lines show the variational estimates for $O_{\rm str}$ ($O_{\rm dim}$).

figure 4(b) is larger as compared with that of (a), and becomes distinct in (c). The difference in figure 4(c) is already clear in the vicinity of $J_2=1$, and persists until $J_2\to-\infty$. The

variation can explain the behaviour of the order parameters only qualitatively in this plot. For example, $O_{\rm str}(J_2)$ is almost independent of J_2 in the region $J_2 < 1$.

Looking at figures 3 and 4, we notice that the convergence to the Haldane state becomes faster as J_1 increases from 0 to 1. For example, $O_{\rm str}(J_2)$ for figure 4(c) takes a value appropriate to the Haldane state even in the isotropic ladder model ($J_2 = 0$). This evidence may allow us to consider that the ground state of the isotropic ladder model is more like the Haldane state than the dimer state.

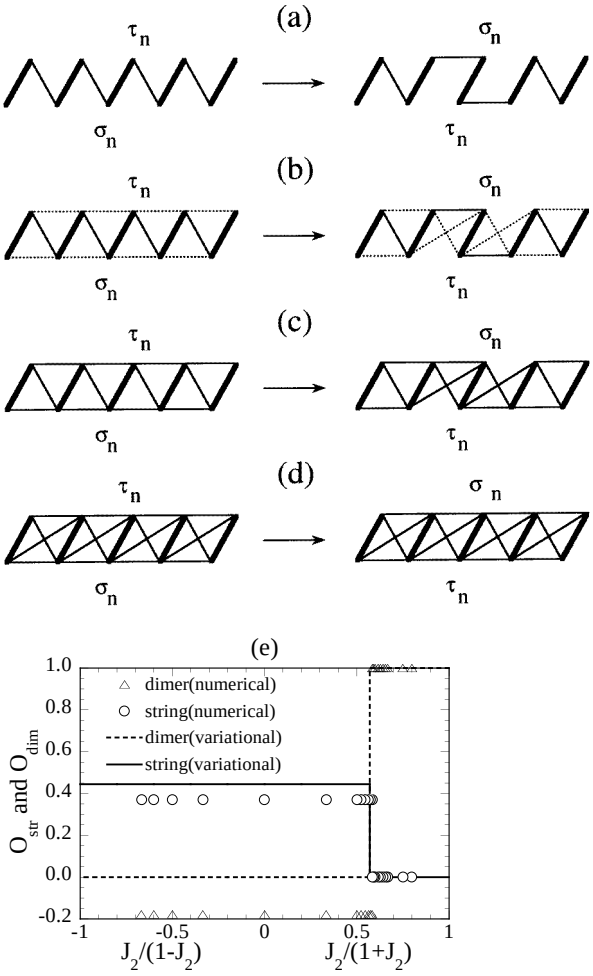

Figure 5. The symmetry of the model with respect to the spin exchange of $\boldsymbol{\sigma}_n$ and $\boldsymbol{\tau}_n$ for (a) $J_1 = 0$, $J_3 = 1$, (b) $J_1 = 0.5$, $J_3 = 1$, (c) $J_1 = 1$, $J_3 = 1$, and (d) the ladder model with both interaction bonds diagonal. Bold lines denote the J_2-bond, thin lines denote the bonds with magnitude 1, and broken lines denote those with magnitude 0.5. (e) The string and the dimer order parameters of model (d).

We relate this tendency to the symmetry of the model with respect to the exchange of two spins that couple to form the $S = 1$ state in the Haldane limit. In general, this spin-exchange symmetry is necessary to realize the Haldane state, since each $S = 1$ unit should have this symmetry. Figure 5 shows a consequence of an exchange of the spins

$\boldsymbol{\sigma}_n$ and $\boldsymbol{\tau}_n$ for the three models that we have considered in this paper. Bold lines denote the J_2-bonds, thin lines denote the bonds of magnitude 1, and broken lines denote those of magnitude 0.5. These models only have this symmetry in the limit of $J_2 \to \pm\infty$, and thus the Haldane state becomes the exact state only in this limit. However, the number of bonds that are invariant before and after this operation increases as J_1 increases from 0 to 1. In this sense, case (c), where $J_1 = 1$ and $J_3 = 1$, is closer to the spin-exchange symmetry.

On the other hand, the ladder model with both interactions diagonal as depicted in figure 5(d) has this symmetry for arbitrary J_2-values. As shown in figure 5(e), the first-order transition from the dimer phase to the Haldane phase occurs at $J_2 = 1.401\,48$ [15]. In this figure, the symbols denote the numerical results for a system with 20 spins. Negative values of the dimer order constitute the finite-size effect. Therefore, we conclude that the convergence to the Haldane state becomes faster as the system gains this spin-exchange symmetry. At the same time, our variational estimates fail more quickly.

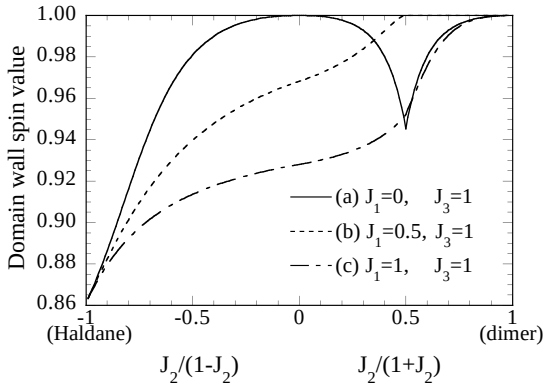

Figure 6. The variational estimates of the spin expectation of a domain wall in the excited state are plotted against $J_2/(1-J_2)$ for $J_2 < 0$, and against $J_2/(1+J_2)$ for $J_2 > 0$, where (a) $J_1 = 0$ and $J_3 = 1$ (the bond-alternation model), (b) $J_1 = 0.5$ and $J_3 = 1$ (including the M–G model at $J_2 = 1$), and (c) $J_1 = 1$ and $J_3 = 1$ (including the isotropic ladder model at $J_2 = 0$).

3. The excited state

The elementary excitation in one dimension is intrinsically a state with one domain wall between the degenerate ground states. Within the present variational scheme, we consider the following one-domain-wall state under open boundary conditions:

$$|\Psi_1\rangle = \sum_i C_i \left(\prod_{n=1}^{i} |n(\alpha, \beta, \gamma, b)\rangle \prod_{n=i+1}^{N} |n(\alpha', \beta', \gamma', b)\rangle \right) \equiv \sum_i C_i \psi_i. \tag{19}$$

Here, the parameter sets (α, β, γ) and $(\alpha', \beta', \gamma')$ are any two of the four possible choices given in equation (12), and b is determined by equation (13). For example, we use the sets $(\alpha, \beta, \gamma) = (\sqrt{2/3}, \sqrt{1/3}, 0)$ and $(\alpha', \beta', \gamma') = (-\sqrt{2/3}, \sqrt{1/3}, 0)$. Of course, the choice does not affect the final results. A domain wall is located between the ith site and the $(i+1)$th site. This definition of the trial function becomes equivalent to the solitonic excitation of Fáth and Sólyom [28] in the AKLT model [29]. The spin expectation of the

domain wall is defined by

$$\langle\psi_i|\boldsymbol{\tau}_i\cdot\boldsymbol{\sigma}_{i+1}+\frac{3}{4}|\psi_i\rangle=\frac{b^2}{9}(b+\sqrt{3(1-b^2)})^2+\frac{3}{4}=\frac{1}{4}O_{\mathrm{dim}}+\frac{3}{4}. \tag{20}$$

Figure 6 shows the J_2-dependence of this value for the three different cases discussed in the previous section. The excitation becomes a local triplet at the domain wall when the ground state is exactly the singlet dimer state. As the ground state changes to the Haldane state, the local triplet smears out, and consequently the local spin value at the domain wall decreases, since the total spin of the excited state is always 1 in this system. In the Haldane limit, it takes a value of $31/36\sim 0.861$.

The basis relations and the matrix element of the Hamiltonian are calculated as

$$\langle\psi_i|\psi_j\rangle=\left(1-\frac{4}{3}b^2\right)^{|i-j|}\equiv(-a)^{|i-j|} \tag{21}$$

$$\langle\psi_i|\mathcal{H}|\psi_j\rangle=[E_{\mathrm{g}}+(|i-j|-1)E_1]\langle\psi_i|\psi_j\rangle+\delta_{ij}[E_1+E_2] \tag{22}$$

with

$$E_{\mathrm{g}}=\epsilon_0 N \tag{23}$$

$$E_1=\frac{-b^2}{3}\left\{(8b^2-4)J_1+\left[\frac{6ab+(b+\sqrt{3(1-b^2)})^5}{(b+\sqrt{3(1-b^2)})^3}-1\right]J_3\right\} \tag{24}$$

$$E_2=\frac{4b^2}{9}\left[6aJ_1+(b+\sqrt{3(1-b^2)})^2J_3\right]. \tag{25}$$

The variation $\langle\Psi_1|\mathcal{H}|\Psi_1\rangle/\langle\Psi_1|\Psi_1\rangle$ can be calculated by Fourier transformation, $|\phi_k\rangle=\sum_n\exp[\mathrm{i}kn]|\psi_n\rangle$, since the denominator $\langle\Psi_1|\Psi_1\rangle$ is diagonalized in the thermodynamic limit. Then the energy gap is obtained with respect to the wavenumber of the domain wall k as

$$\begin{aligned}E_{\mathrm{ex}}(k)&=\frac{\langle\phi_k|\mathcal{H}|\phi_k\rangle}{\langle\phi_k|\phi_k\rangle}-E_{\mathrm{g}}\\&=-E_1\left[1+\frac{2a}{1-a^2}\frac{(1+a^2)\cos k+2a}{1+2a\cos k+a^2}\right]+(E_1+E_2)\frac{1+2a\cos k+a^2}{1-a^2}\end{aligned} \tag{26}$$

where a is defined by equation (21).

We plot this estimate with $k=0$ and $k=\pi$ in figure 7, and compare it with the numerical results.

In the vicinity of the M–G point, $(J_1,J_2,J_3)=(0.5,1,1)$, the lowest excitation is a kink–antikink state, which consists of $N-1$ singlet dimer pairs and two free $S=1/2$ spins [3]. We call these free spins a kink and an antikink. In such a case, we try another variation. These two free spins are mobile in general, and thus we have to consider the following trial function:

$$|\psi_{ij}\rangle=\prod_{n=1}^{i-1}|n(0)\rangle\prod_{n=i}^{j-1}|n(\alpha,\beta,\gamma,b)\rangle\prod_{n=j}^{N}|n(0)\rangle \tag{27}$$

under periodic boundary conditions. Here, $|n(0)\rangle$ stands for the singlet dimer state on the $\boldsymbol{\sigma}_n$–$\boldsymbol{\tau}_n$ bond with $b=0$. $|n(\alpha,\beta,\gamma,b)\rangle$ becomes another singlet dimer state on the $\boldsymbol{\sigma}_{n+1}$–$\boldsymbol{\tau}_n$ bond when $b=\sqrt{3}/2$ at the M–G point. Therefore a kink or an antikink should exist at the domain wall.

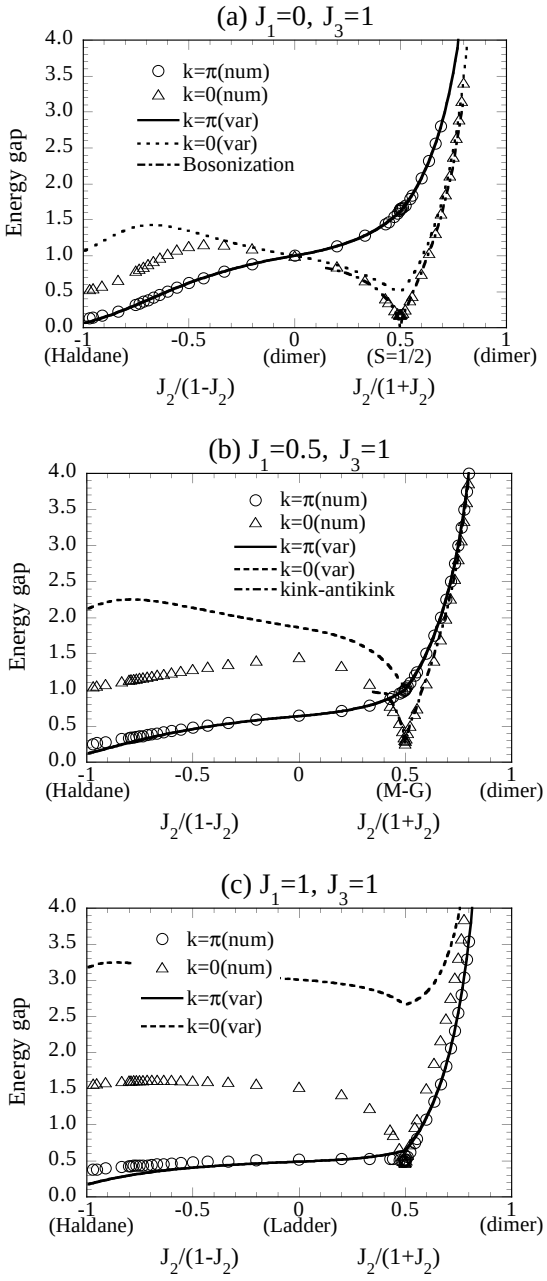

Figure 7. The J_2-dependence of the energy gap obtained by the numerical diagonalization (symbols), and the variation (lines) plotted against $J_2/(1-J_2)$ for $J_2 < 0$, and against $J_2/(1+J_2)$ for $J_2 > 0$, where (a) $J_1 = 0$ and $J_3 = 1$ (the bond-alternation model), (b) $J_1 = 0.5$ and $J_3 = 1$ (including the M–G model at $J_2 = 1$), and (c) $J_1 = 1$ and $J_3 = 1$ (including the isotropic ladder model at $J_2 = 0$). We also plot the estimate of the kink–antikink variation (dash–dot line) in (b).

In the Δ chain, a kink becomes localized, and thus the problem can be reduced to a one-body problem of a moving antikink. We can solve it exactly, and the wave function is

given by the Airy function [26, 27]. Here, we solved this variation only numerically for a finite system with $N = 30$. The results are also plotted in figure 7(b) as a dash–dot line.

The relative motion of this two-body problem is the same as that of the one-body problem of the Δ chain. That is, we obtain the same equation if we set one free spin at the origin and rewrite the variational problem with respect to the one-body problem of the other free spin. This is also verified by the fact that the wave function obtained numerically is well fitted by the Airy function, and that the gap enhancement, $E_{\rm gap}(J_2) - E_{\rm gap}(J_2 = 1)$, is almost equal to that of the Δ chain; it obeys a power law with exponent $2/3$ [26, 27, 30]. Of course, the gap itself cannot be obtained correctly from just the relative motion; the motion of the centre of mass also has to be taken into account.

Figure 7 shows the J_2-dependence of the energy gap estimated above for the cases with (a) $J_1 = 0$, $J_3 = 1$, (b) $J_1 = 0.5$, $J_3 = 1$, and (c) $J_1 = 1$, $J_3 = 1$. The local triplet excitation with $k = \pi$ is depicted by solid lines, that with $k = 0$ is depicted by broken lines, and the kink–antikink excitation is depicted by a dash–dot line in figure 7(b). The lowest gap in the $k = \pi$ sector and that in the $k = 0$ sector calculated by the numerical diagonalization of an $N = 12$ lattice are depicted by circles and by triangles, respectively. The variational estimates with $k = \pi$ are quite excellent for all of the plots. We consider that this is because the local approximation is usually good for the wavenumber π, which changes the phase of the wave function by only one lattice spacing. The only difference is that the local triplet variation converges to the VBS value in the $J_2 \to -\infty$ limit, while the numerical one converges to the Haldane value. When the ground state is the exact singlet dimer state ($J_2 > J_3 = 1$ in figure 7(b)), our variational excitation is a local triplet state, and thus the gap value is equal to J_2 with no dispersion. On the other hand, the estimates with $k = 0$ only explain the gap behaviour qualitatively, and become worse with an increase of J_1. They are only valid near the pure dimer points in figure 7(a). In the vicinity of the gapless point where $J_2 = J_3 = 1$ (the $S = 1/2$ chain), our variational scheme breaks down, and thus the gap estimation should be done by another method. For example, the bosonization technique [31–33] gives

$$\frac{1}{2}\left(\frac{18}{\pi}\right)^{1/3}\frac{|2x-1|^{2/3}}{1-x} \tag{28}$$

with $x = J_2/(1 + J_2)$, and agrees with our numerical results very well. This is plotted as a dash–dot line in figure 7(a). The variational estimate of kink–antikink type is also consistent with the numerical results. We can consider that it is valid as long as the singlet dimer state is exactly or approximately the ground state.

4. Summary and discussion

We have investigated the general $S = 1/2$ double-spin-chain (J_1–J_2–J_3) model by means of a non-local unitary transformation and a variational method. The model includes the dimer model and the Haldane system as its two extremes. A ground-state change occurs at the symmetric point, $J_2 = J_3 = 1$, as is manifested by the string and the dimer order parameters. The ground state for $J_2 < J_3$ continuously changes to the Haldane state in the $J_2 \to -\infty$ limit, and the other ground state, for $J_2 > J_3$, becomes the dimer state in the $J_2 \to \infty$ limit. The two states are degenerate at the symmetric point.

We relate the convergence to the Haldane state to the symmetry of the exchange of spins that will couple to the $S = 1$ state in the Haldane limit. As the system gains some of this symmetry, the convergence of the ground state to the Haldane state becomes faster, or,

in other words, the transition becomes close to a first-order one. In the case of the system with full symmetry, the transition is strictly of first order [15].

The excited state is formulated in terms of a domain wall between two of the fourfold-degenerate ground states. In the dimer region, this domain wall is equivalent to a local triplet. We obtained an explicit form for the dispersion relation of the gap for arbitrary J_1, J_2, and J_3. That is, we first calculate the value of b by means of equation (13) for a given (J_1, J_2, J_3). Then, the dispersion is given by equation (26) with $a = 4/3b^2 - 1$. We confirmed that our variational estimate is generally good in the dimer region, $J_2 > J_3$, and is especially excellent for the excited state with $k = \pi$. The lowest excitation near the M–G point is well explained by a kink–antikink state [3, 26, 27].

Our variation employs the single-site approximation in the transformed system, which of course becomes worse when the ground state has a rather long correlation length, e.g. as in the Haldane state. Therefore, our estimate fails more quickly with the convergence to the Haldane system. We must go beyond the single-site approximation for the sake of quantitative agreements in this region.

Finally, we point out the possibility that the ground state of a real compound is stabilized by a lattice dimerization to the dimer state, since its energy stabilization is quite significant, as we observed in figure 2. In fact, the susceptibility of $KCuCl_3$ is quantitatively explained by a single-dimer model with $J = 48.8$ K [20]. The situation is similar in the case of CaV_2O_5 [18].

Acknowledgments

The authors would like to thank M Onoda and H Tanaka for valuable discussions. They also acknowledge H Nishimori for supplying his diagonalization package, Titpack Version 2. The computations were performed partly on Facom VPP500 at the ISSP, University of Tokyo.

References

[1] See, for example,
Dagotto E and Rice T M 1996 *Science* **271** 618
[2] Majumdar C K and Ghosh D 1969 *J. Math. Phys.* **10** 1388
[3] Shastry B S and Sutherland B 1981 *Phys. Rev. Lett.* **47** 964
[4] Kubo K 1993 *Phys. Rev.* B **48** 10 552 and references therein
[5] Nakamura T and Kubo K 1996 *Phys. Rev.* B **53** 6393
[6] Sen D, Shastry B S, Walstedt R E and Cava R 1996 *Phys. Rev.* B **53** 6401
[7] Haldane F D M 1983 *Phys. Rev. Lett.* **50** 1153
[8] For a review, see
Hida K 1995 *Computational Physics as a New Frontier in Condensed Matter Research* ed H Takayama *et al* (Tokyo: The Physical Society of Japan) p 187 and references therein
[9] Takada S and Watanabe H 1992 *J. Phys. Soc. Japan* **61** 39
[10] Narushima T, Nakamura T and Takada S 1995 *J. Phys. Soc. Japan* **64** 4322
Hida K 1995 *J. Phys. Soc. Japan* **64** 4896 and references therein
[11] Nishiyama Y, Hatano N and Suzuki M 1995 *J. Phys. Soc. Japan* **64** 1967
[12] Hida K 1992 *Phys. Rev.* B **45** 2207
[13] Takada S 1992 *J. Phys. Soc. Japan* **61** 428
[14] Hida K and Takada S 1992 *J. Phys. Soc. Japan* **61** 1879
[15] Kitatani H and Oguchi T 1996 *J. Phys. Soc. Japan* **65** 1387
[16] Ramirez A P 1994 *Annu. Rev. Mater. Sci.* **24** 453
[17] Tanaka H, Takatsu K, Shiramura W and Ono T 1996 *J. Phys. Soc. Japan* **65** 1945
[18] Onoda M and Nishiguchi N 1996 *J. Solid State Chem.* **127** 358
[19] Takatsu K, Shiramura W and Tanaka H 1997 *Preprint*

[20] Nakamura T and Okamoto K 1997 in preparation
[21] See, for example,
Troyer M, Tsunetsugu H and Würtz D 1994 *Phys. Rev.* B **50** 13 515
[22] den Nijs M and Rommelse K 1989 *Phys. Rev.* B **40** 4709
[23] Brehmer S, Mikeska H-J and Neugebauer U 1996 *J. Phys.: Condens. Matter* **8** 7161
[24] Kennedy T and Tasaki H 1992 *Phys. Rev.* B **45** 304
[25] Takada S and Kubo K 1991 *J. Phys. Soc. Japan* **60** 4026
[26] Nakamura T and Takada S 1997 *Phys. Rev.* B **55** at press
[27] Nakamura T and Takada S 1997 *Phys. Lett.* **225A** 315
[28] Fáth G and Sólyom J 1993 *J. Phys.: Condens. Matter* **5** 8983
[29] Affleck I, Kennedy T, Lieb E and Tasaki H 1987 *Phys. Rev. Lett.* **59** 799
Affleck I, Kennedy T, Lieb E and Tasaki H 1988 *Commun. Math. Phys.* **115** 477
[30] Chitra R, Pati S, Krishnamurthy H R, Sen D and Ramasesha S 1995 *Phys. Rev.* B **52** 6581
[31] Nakano T and Fukuyama H 1980 *J. Phys. Soc. Japan* **49** 1679
[32] Okamoto K 1996 *J. Phys. A: Math. Gen.* **29** 1639
[33] Okamoto K and Nakamura T 1997 *Preprint*